JOURNAL OF MATERIALS SCIENCE 28 (1993) 4749–4761

The effects of matrix microcracking on the oxidation behaviour of carbon-fibre/glass-matrix composites

R. G. IACOCCA*, D. J. DUQUETTE
Department of Materials Engineering, Rensselaer Polytechnic Institute, Troy, NY 12180-3590, USA

Carbon-fibre/glass-matrix composites were fabricated using Fortafil fibres and two different glass matrices: a sodium-borosilicate glass (CGW 7740), and a calcium-aluminosilicate glass (CGW 1723). Upon cooling from the hot-pressing temperature used to fabricate the composites (approximately 1250 °C), the glass matrices cracked due to differences in the coefficients of thermal expansion between the fibres and the matrix. At elevated temperatures these cracks serve as short-circuit diffusion paths for oxygen transport, and the majority of the weight loss from the cracked samples was caused by oxygen diffusing along these microcracks and reacting with the fibres. Because of the relatively large diameter of these cracks compared to the mean free path for diffusing oxygen, traditional gas kinetics can be applied to the various transport processes occurring in the oxidation reactions, and there is no need to allow for capillary size or to apply Knüdsen diffusion. The composites made of 1723 glass exhibited linear relationships between specific-mass loss (Δ mass/initial exposed surface area of carbon fibres) and time at all oxidation temperatures (450, 500, 550 and 600 °C). With the 7740 composites, a parabolic relationship between specific-mass loss and time was obtained. As the oxidation temperature approached or exceeded the glass-transition temperature, T_g, for the 7740 composites (560 °C), this parabolic relationship became more pronounced. Microstructural evidence revealed that at temperatures near or exceeding the T_g for the 7740 glass the microcracks in the matrix heal, thereby decreasing the amount of fibre surface area available for chemical reaction. Because the rate of oxidation is directly proportional to the amount of available fibre-surface area, the weight-loss data appear parabolic with time. Additionally, the mechanism for the oxidation of the carbon fibres does not appear to change once the fibres are placed in a glass matrix. The apparent activation energy for oxidation remained constant at approximately 174 kJ mol^{-1}.

1. Introduction

Since the 1960s, the beneficial aspects of carbon-fibre/glass-matrix composites have been recognized. Their properties of low density, high modulus, and high specific strength have made them candidates for a number of different industrial applications. The first people to recognize the desirable properties of carbon-fibre/glass-matrix materials were Crivelli-Visconti and Cooper [1]. Using pure silica as a matrix material, they were able to produce composite materials with up to 50 vol % carbon fibres. Unfortunately, silica does not have a suitable processing viscosity until temperatures of approximately 1800 °C. Because of this, the composites made in this research effort were rather porous. Additionally, the carbon fibres reacted with the silica, creating a very strong fibre/matrix interface; therefore, the composite lacked the toughness necessary to be considered as a viable industrial material.

Beginning in the early 1970s, a renewed interest was taken in carbon-fibre/glass-matrix composites, this time using Pyrex glass as a matrix material [2–4]. At temperatures above 500 °C, however, the glass did not act as a protective barrier to oxygen transport, and the fibres were severely degraded.

Promising results were obtained when the matrix material was changed to lithium-aluminosilicate glasses [5]. Mechanical testing at room temperature showed a weak bond at the fibre/matrix interface, evinced by crack deflection parallel to the fibre axis. Thermal cycling between room temperature and 1200 °C produced no adverse effects on the mechanical properties.

Since these early efforts, the vast majority of research on carbon-fibre/glass-matrix composites has been conducted at major US corporations such as Corning Glass and the United Technologies Research Center due to the intense research efforts required to

* Currently a Research Assistant in the Department of Engineering Science and Mechanics, The Pennsylvania State University, University Park, PA 16802, USA.

successfully produce these materials. Several review articles have been published which provide a more in-depth look at the overall development of composite materials [6–8].

Despite the attractive properties of these materials, several phenomena must be understood before they can be used as industrial components, such as their oxidation properties. Upon cooling from the hot-pressing temperature, the matrix invariably cracks due to differences in the coefficients of thermal expansion between the fibres and the glass. These cracks may play a significant role in the oxidation of the composites by serving as short-circuit transport paths by which oxygen can gain access to the fibres. The purpose of this investigation was to characterize the thermo-oxidative stability and to determine the effects of matrix microcracks on the oxidation behaviour of carbon-fibre/glass-matrix composite materials.

2. Materials characterization

2.1. Carbon fibres

All the PAN-based 5C carbon fibres used in this investigation were provided by Fortafil Fibers, Inc., a subsidiary of Akzo International. The fibres were received on three large spools, with each spool containing a "tape" of fibres, which was four fibre tows (50 000 filaments per tow) wide (approximately 100 mm) and 60 m long. Table I shows a list of fibre properties.

Fig. 1 shows a micrograph of the fibres taken by scanning electron microscopy (SEM) of the fibre surface. The surface exhibits a fluted or ribbed topographical structure. If the fibres are examined end on, an onion-skin structure can be seen on the outside of the fibres (Fig. 2). This is typical for PAN-based fibres [9, 10]. Actual values for the thickness of the onion skin range from 0.1 μm to in excess of 1 μm [11–12]. Analysis of the fibres using X-ray diffraction (XRD) produced one broad peak occurring at a value of 2θ for (0 0 0 2) hexagonal-graphite planes indicating that only a portion of the fibre is graphitic. This is consistent with the skin–core heterogeneity, as the fibre skin of PAN-based fibres is comprised of partially graphitic carbon, while the core is amorphous.

The fibres were also examined using a scanning auger microprobe. Trace amounts of sodium and chlorine were detected on the surface of the fibres; however, sputtering the surface for approximately 2 min at an accelerating voltage of 5 kV removed all evidence of these elements.

2.2. Glass matrices

Two different glasses were used as matrix materials:

TABLE I Properties of Akzo 5C Fortafil Fibres

Tensile strength (MPa)	2760
Tensile modulus (GPa)	345
Ultimate elongation (%)	0.8
Density (kg m^{-3})	1800
Filament shape	Round
Filament diameter (μm)	7

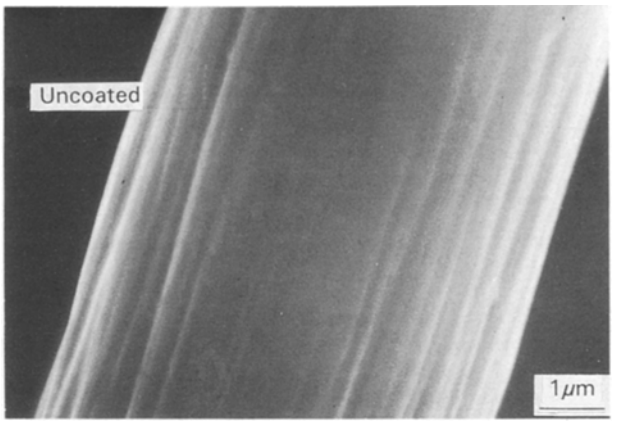

Figure 1 Scanning electron micrograph of Akzo fibres showing a ribbed or fluted surface.

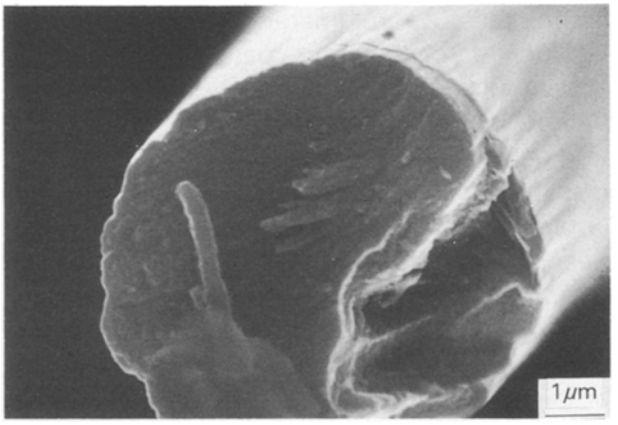

Figure 2 Scanning electron micrograph of a fibre in an end-on view showing an onion-skin structure.

CGW 7740, a sodium borosilicate glass (Pyrex); and a calcium aluminosilicate glass with a composition close to that of CGW 1723. The nominal compositions of both the 7740 and 1723 glasses are shown in Table II [13]. The composition for the 1723 glass was slightly modified, due to the availability of necessary compounds. This modified composition is also shown in Table II. As the composition is very close to that of CGW 1723, the modified composition will be referred to as 1723 glass.

The 7740 glass was purchased directly from Corning Glass as a − 325 mesh powder. This particular glass was chosen as a matrix material for three reasons: (i) it is commercially available in powder form, (ii) it has known chemical and mechanical properties, and (iii) its ease of composite fabrication due to its relatively low working point. The particle-size distribution of the as-received powder shown in Fig. 3 was determined using a commercial, light-scattering, particle size analyser. The average particle size is approximately 5 μm.

The CGW 1723 glass is no longer available commercially in cullet or powder form; therefore, the glass was melted and ground into powder using the facilities available at Rensselaer Polytechnic Institute. Oxide and borate powders were weighed out in the appropriate proportions, and mixed in ethanol for several

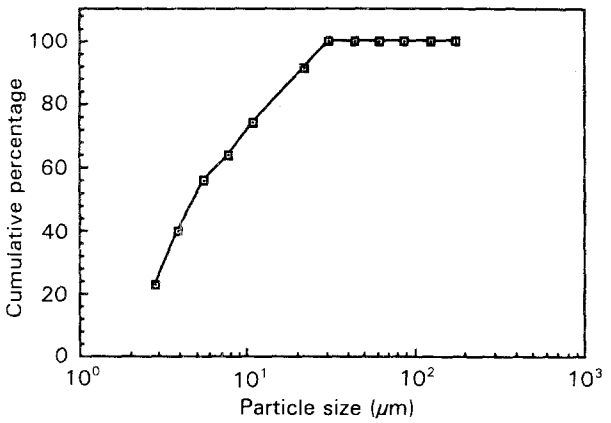

Figure 3 Cumulative particle-size distribution for the as-received CGW 7740, – 325 mesh powder.

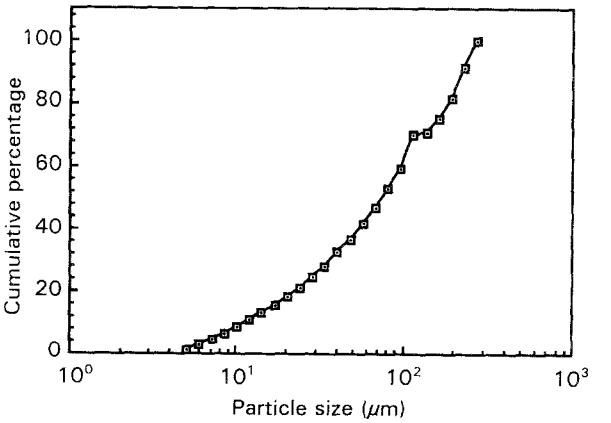

Figure 4 Cumulative particle-size distribution for the as-milled CGW 1723, – 270 mesh powder.

hours. After mixing, the powder was placed overnight in a drying oven to remove excess ethanol. The agglomerated powder was broken up and placed in a platinum crucible (100 ml capacity), which was subsequently heated to approximately 1500 °C. As the powder melted, additional powder was added to the crucible. After the crucible was at capacity, the glass was allowed to soak at 1600 °C to remove any residual gas bubbles. The glass was then poured on to a brass plate. (No stress-relieving anneal was given as the cullet was to be milled into powder and subsequently hot pressed.)

Using a mortar and pestle, the glass was ground into smaller pieces. These pieces were placed in an alumina milling jar containing corundum pellets, milled for approximately 100 h, and powder was sieved to a – 270 mesh. Fig. 4 shows the particle-size distribution for the powder, with the average particle size being approximately 8 μm.

The 1723 glass was chosen as a matrix material mainly for its high glass-transition temperature of 710 °C. As one of the initial overall goals of this investigation was to fabricate composites which could be exposed to temperatures up to 800 °C, it was necessary to use glass matrices that have high glass-transition temperatures. The benefit of choosing the CGW 1723 glass over other high-silica-containing glasses is that although it has a high T_g, the 1723 glass has a working temperature which is approximately the same as Pyrex. Therefore, "green" plies infiltrated with the 1723 powder did not require a higher hot-pressing temperature than those plies infiltrated with the 7740 glass.

3. Composite manufacture

The basic technique used in manufacturing the composites used in this investigation has been described in detail elsewhere [2, 14]. However, as the process had to be modified to accommodate limited amounts of raw materials, the method used in this investigation will be described here.

The fibres were cut to the appropriate length, placed in a metal frame (Fig. 5), and then stretched, thereby aligning the fibres unidirectionally. Infiltration of the

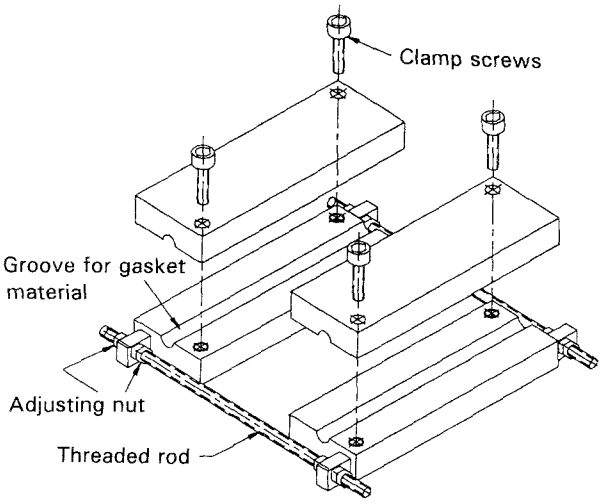

Figure 5 Schematic of the aluminium frame used to hold the fibre tows for glass-powder infiltration and drying.

TABLE II Nominal compositions of glasses used as matrix materials

	Composition (wt %)						
Code	SiO_2	B_2O_3	Na_2O	MgO	CaO	BaO	Al_2O_3
7740	81	13	4	–	–	–	2
1723	57	4	–	7	9	7	16
Modified 1723	61	4	–	7	11	–	17

fibres with the glass was accomplished by pouring a slurry consisting of glass powder, an organic surfactant (Tamol), an organic binder (Rhoplex), and distilled water over the fibres. The exact proportions used in the slurry are given in Table III. To form a ply of the composite, the slurry was poured over each side of the fibre tape for a total of three times. This was sufficient to uniformly infiltrate the fibres with glass powder. Fig. 6 shows a scanning electron micrograph of a green ply infiltrated with 7740 powder. The glass particles are evenly dispersed among the carbon fibres. The frame was then placed under a heat lamp and

TABLE III Composition of slurry

Ingredient	Amount
Glass powder	100 g
Organic binder (Rhoplex)	25 ml
Organic surfactant (Tamol)	~0.5 g
Distilled water	Remainder to make 250 ml of slurry

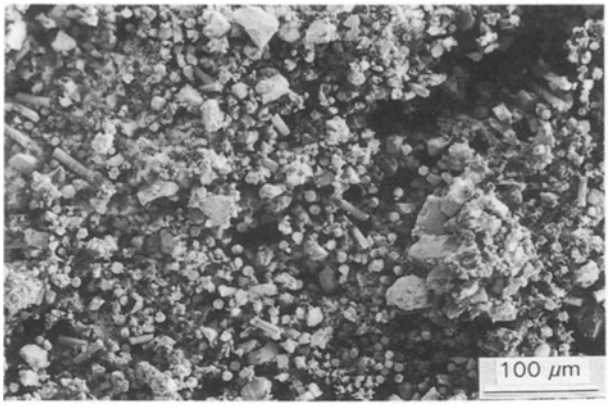

Figure 6 Scanning electron micrograph of an as-infiltrated ply.

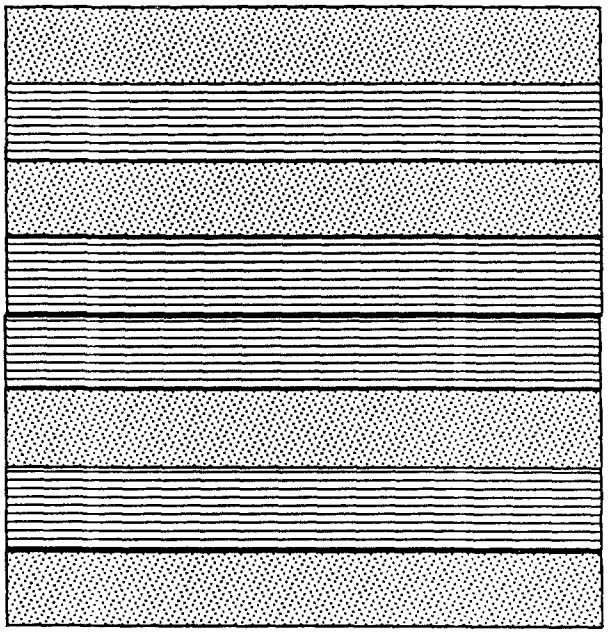

Figure 7 Schematic of the lay-up for cross-plied composites, illustrating a $[0/90]_{2s}$ configuration.

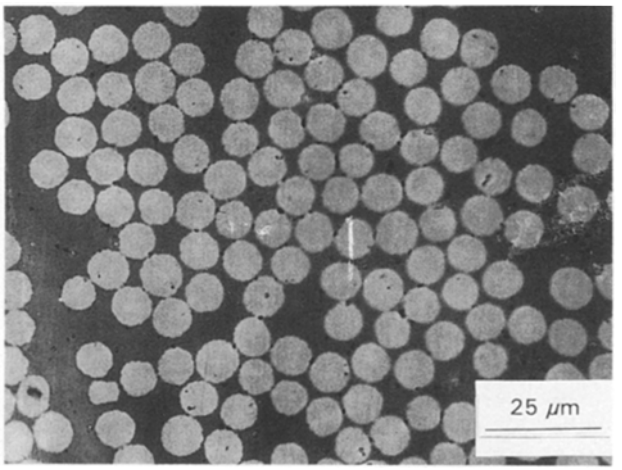

Figure 8 Microstructure of an as-hot-pressed 1723 unidirectional composite.

allowed to dry. By driving off the excess water, the binder gave the infiltrated fibres the necessary stiffness to be handled. Once dry, the ply was removed from the frame and cut to size (76.2 × 76.2 mm). After a sufficient number of glass-infiltrated plies had been manufactured, the plies were hot pressed. In the hot press, the samples were heated (under an inert atmosphere of argon) to approximately 300 °C to burn off the organic binder and surfactant. The temperature was then increased to 1250 °C, and the plies were hot pressed at a pressure of 6.9 MPa for approximately 15 min for final consolidation.

Two different lay-ups were made from each matrix composition: unidirectional and cross-plied $[0/90]_{2s}$. Fig. 7 shows a schematic of the lay-up used for the 0/90° composites. The planar symmetry of the cross-plied lay-up was chosen to prevent warpage in the final hot-pressed material. Seven plies were used to fabricate the unidirectional composites, while eight were used in the $[0/90]_{2s}$ material. The final composites had approximate dimensions of 76.2 × 76.2 × 1.6 mm.

4. Composite characterization and microstructure

Figs 8–11 show micrographs of the four types of composites used in this study: 1723 unidirectional and $[0/90]_{2s}$, and 7740 unidirectional and $[0/90]_{2s}$. Because of the coefficient-of-thermal-expansion (CTE) mismatch between the fibres and glass mentioned previously, the glass matrices did indeed crack. Fig. 12 shows a typical matrix microcrack in a metallographically prepared sample. The cracks are distinguishable from processing defects/voids in that: (i) they are regularly spaced; (ii) they are not spherical in shape; (iii) they originate at the composite edge; (iv) all the composites were processed identically, yet the degree of microcracking varies as a function of lay-up and CTE; and (v) the glass powder fully infiltrated the green plies, as previously shown in Fig. 6.

Additionally, all of the composites were hot pressed at the working point of the glass matrix. The viscosity at this temperature is low enough (10^4 Pa s) to permit the glass to flow around the fibres under a stress of 6.9 MPa.

Quantitative metallographic techniques were used to determine the volume fraction of cracks in each of the four composite materials used in this investigation. Samples of composite material, approximately 6 mm square and 1.6 mm in thickness were sectioned diagonally, mounted in epoxy and polished. After polishing, a photographic montage was taken of the exposed surface. The photographs were trimmed and weighed on an analytical balance. Using a surgical

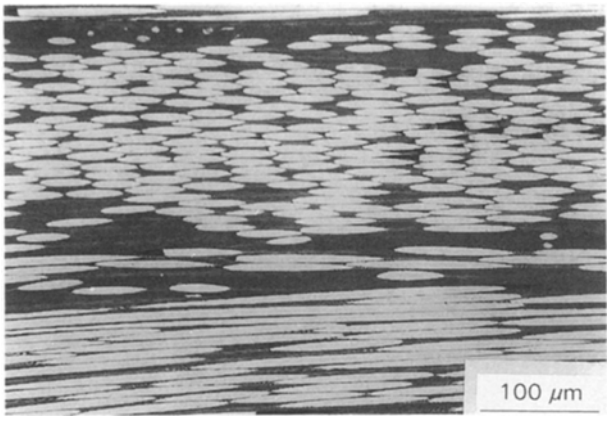

Figure 9 Microstructure of an as-hot-pressed 1723 $[0/90]_{2s}$ composite.

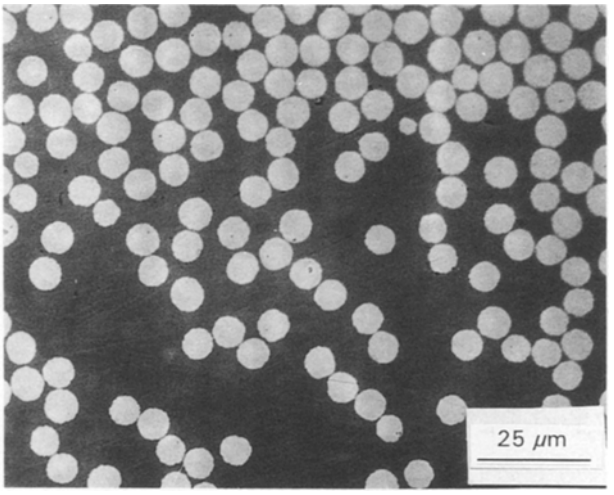

Figure 10 Microstructure of an as-hot-pressed 7740 unidirectional composite.

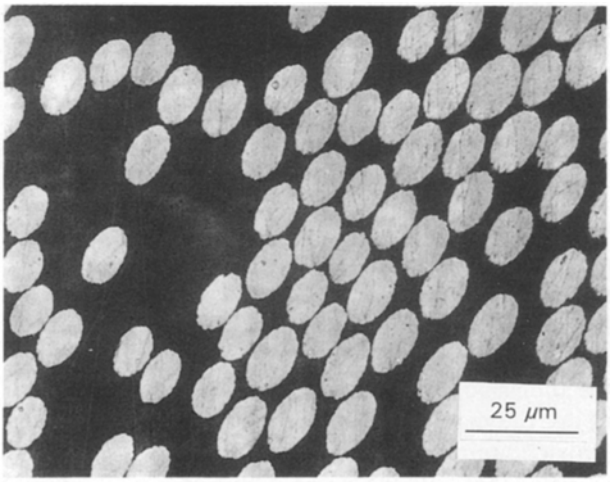

Figure 11 Microstructure of an as-hot-pressed 7740 $[0/90]_{2s}$ composite.

scalpel, the cracks were carefully cut out of the photographs, after which the photographs were reweighed. The volume fraction of cracks was calculated by dividing the difference in weight between the uncut and cut photographs by the total weight of the photographs in the uncut condition. Table IV shows the

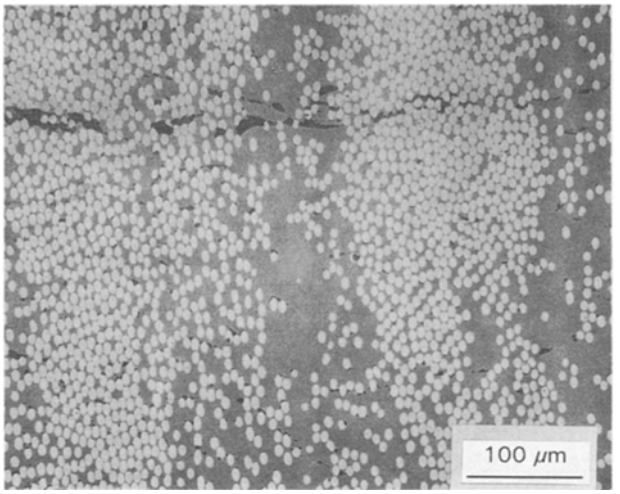

Figure 12 Micrograph of a typical matrix microcrack.

TABLE IV Volume fraction of microcracks

Composite	Volume fraction (%)
Unidirectional 7740	0
$[0/90]_{2s}$ 7740	3.8 ± 0.8
Unidirectional 1723	0.6 ± 0.4
$[0/90]_{2s}$ 1723	1.2 ± 0.8

TABLE V The as-hot-pressed density of composites

Composite	Experimental Density ($kg\ m^{-3}$)
Unidirectional 7740	2070
$[0/90]_{2s}$ 7740	2071
Unidirectional 1723	2229
$[0/90]_{2s}$ 1723	2262

TABLE VI Volume fraction of fibres

Composite	Volume fraction (from density measurements)	Volume fraction (from quantitative microscopy)
Unidirectional 7740	0.37	–
$[0/90]_{2s}$ 7740	0.37	0.40
Unidirectional 1723	0.49	–
$[0/90]_{2s}$ 1723	0.45	0.42

volume fraction of microcracks for the four composites. As the microcracks in the unidirectional 7740 material were not visible at the chosen magnification, this material was assigned a crack volume fraction of zero.

Composite densities were determined using an application of Archimedes' principle (ASTM B328). The results are shown in Table V. If the densities of the fibres and the glass used for the matrix are known and it is assumed that the density of the composites follows a rule-of-mixtures relationship, the volume fraction of fibres for each material can be calculated, as shown in Table VI. To verify these values, the fibre-volume

fraction was calculated using quantitative metallographic technics on the two $[0/90]_{2s}$ composites. The results from this technique are also shown in Table V. As the values are within several per cent of the numbers obtained using Archimedes' principle, only two composites were analysed by this method.

5. Experimental procedure

All fibre and composite samples were tested in atmospherically controlled, single-zone tube furnaces. The sample to be oxidized was placed in a silica fixture which consisted of a longitudinal cross-section of a quartz tube. (Silica was chosen for the specimen holder because it does not catalyse carbon, as many other materials do.) The sample and quartz fixture were the placed in an alumina boat, which was then placed in the centre of the hot zone. At periodic times, the samples were removed and weighed. The composite samples were removed from the silica holder, while the fibres remained in the holder to prevent the fibres from being damaged and/or scattered. Both the fibres and the composites were oxidized at 500, 550 and 600 °C. Additional composite samples were oxidized at 450 °C.

6. Results and discussion

6.1. Oxidation of carbon fibres

Fig. 13 shows the data collected from the carbon fibres which were oxidized at 500, 550 and 600 °C in dry air. The data are plotted as change in mass, normalized by the initial exposed surface area (specific-mass loss) against time. As the reaction between carbon and oxygen takes place on the surface of the fibres, it is reasonable to normalize the changes in mass by the initial surface area of the fibres, where surface area is defined as $2\pi r_0 l_0 + 2\pi r_0^2$, with r_0 equal to the initial radius (7 μm) and l_0 equal to the initial length of the fibres (5 cm, all fibre oxidation samples were cut to this length). Knowing the fibre dimensions, mass, and density, the number of fibres in each oxidation sample was determined, and the surface area was then calculated.

The slopes of the lines shown in Fig. 13 are the effective oxidation rates for the fibres at that temperature. As oxidation is a thermally activated process, it is reasonable to assert that this rate of reaction follows a classical Arrhenius relationship:

$$R_T = A\exp(-Q/RT) \quad (1)$$

where: R_T is the rate of reaction at temperature, T; Q is the effective activation energy for the oxidation of carbon fibres; T is temperature (K); R is the ideal gas constant; and A is a pre-exponential term. If the slopes of the lines shown in Fig. 13 are plotted on semi-logarithmic axes with T^{-1} as the dependent variable, the slope of the resulting line is $-Q/R$ (Fig. 14). The effective activation energy for the oxidation of Akzo carbon fibres was determined to be 176.6 kJ mol^{-1}. This value is consistent with the activation energies for the oxidation of other PAN-based fibres [15–17].

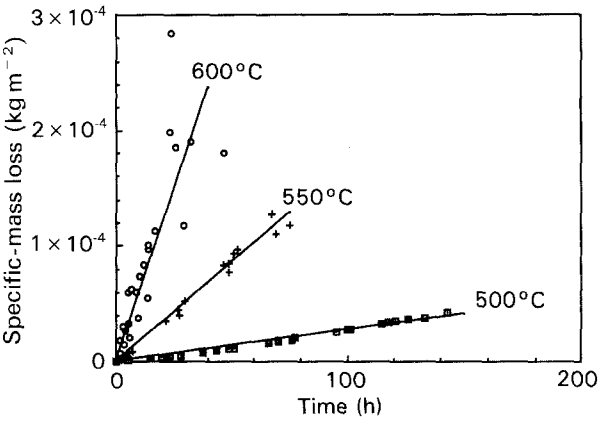

Figure 13 Oxidation data from carbon fibres oxidized at 500, 550 and 600 °C in dry air. Specific-mass loss (Δ mass/initial surface area) is plotted against time.

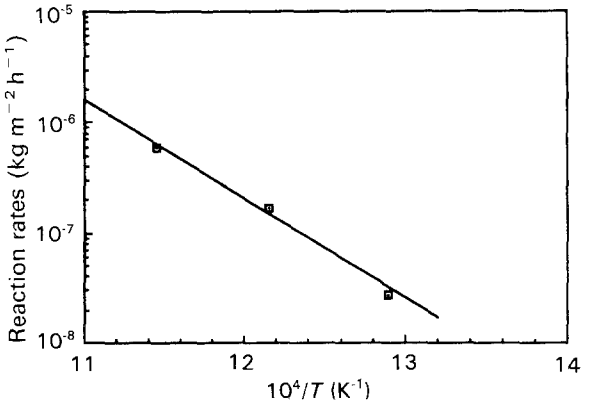

Figure 14 Plot of log(reaction rate) versus T^{-1} showing an Arrhenius relationship for the oxidation rate of carbon fibres in dry air.

6.2. Oxidation of carbon-fibre/glass-matrix composites

The data obtained in the oxidation of the unidirectional 1723 composites are shown in Fig. 15. The line drawn for each temperature was calculated using a linear least-squares analysis, and appears to describe accurately the relationship between specific-mass loss and time.

The normalizing surface area for the composites was calculated in a different way to the bare fibres. The composite oxidation samples were all cut to the same approximate dimensions, 12.5 × 12.5 × 1.6 mm. Knowing the volume fraction of fibres for each of the composite materials, the dimensions of each sample, the dimensions of the fibres, and the density of the fibres, the mass and number of fibres was calculated for each sample. With the composites, however, it was assumed that only the exposed fibre ends would participate in the oxidation process. Thus, the normalizing surface area was determined by multiplying the number of fibre ends (double the number of fibres) by the surface area of a single fibre end, $\pi(r_0)^2$, where r_0 is the initial fibre radius (7 μm). This convention was used for all the composite data.

As with the bare fibres, it is reasonable to assert that the rate of oxidation of the carbon fibres contained within the 1723 matrix follows an Arrhenius-type

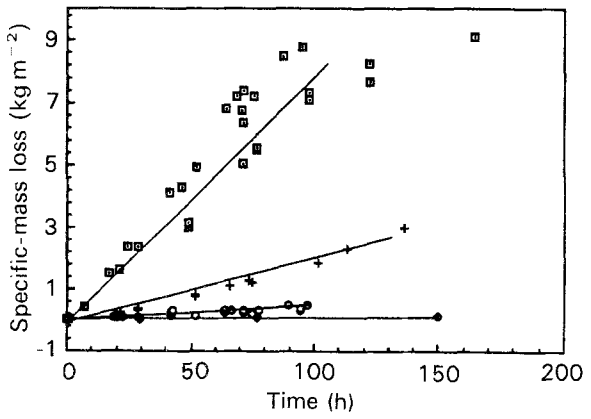

Figure 15 Plot of specific-mass loss versus time for 1723 unidirectional composites oxidized in dry air at: (□) 600 °C, (+) 550 °C, (○) 500 °C, and (◇) 450 °C.

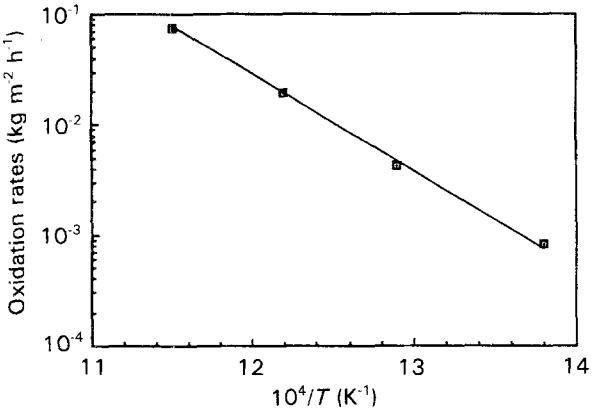

Figure 16 Semi-log plot of the reaction rate versus T^{-1} showing an Arrhenius-type relationship for the oxidation rates of fibres in 1723 unidirectional composites.

relationship. Thus, a plot of the logarithm of the slopes of the lines shown in Fig. 15 against T^{-1} should produce a straight line whose slope is equal to $-Q/R$, where Q is the effective oxidation activation energy for the fibres contained in the 1723 matrix. This plot is shown in Fig. 16, with the activation energy being 174 kJ mol^{-1}. This value is consistent with the activation energy for the bare carbon fibres.

Fig. 17 shows a plot of specific-mass loss versus time for $[0/90]_{2s}$ 1723 composites oxidized at 450, 500, 550, and 600 °C in dry air. As with the unidirectional 1723 composites, the mathematical relationship between specific-mass loss and time is adequately described by a linear least-squares fit. In plotting the slopes of these best-fit lines as log(slopes) against T^{-1}, the effective activation energy for the oxidation of the $[0/90]_{2s}$ 1723 composites was determined to be 174 kJ mol^{-1}, which is in agreement with the calculated activation energy for the unidirectional 1723 composites and the bare Fortafil fibres.

In addition to having the same effective oxidation activation energy, both the unidirectional and $[0/90]_{2s}$ 1723 composites have the same oxidation rate. Fig. 18 shows a comparison of the unidirectional and cross-plied composite oxidation data for 450, 500, 550, and 600 °C. All the data seem to fall within the bounds of experimental scatter at each temperature. In all instances, there is no distinction in the oxidation data

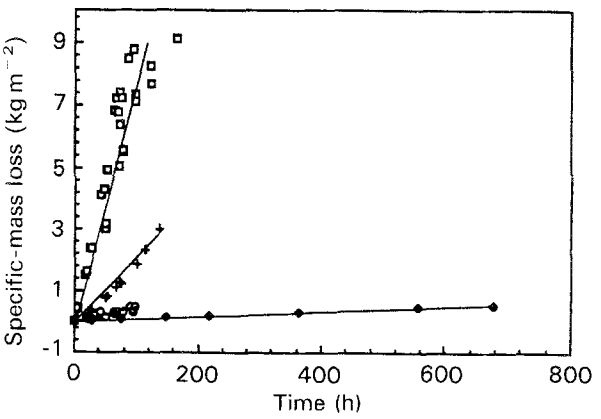

Figure 17 Plot of specific-mass loss versus time for 1723 $[0/90]_{2s}$ composites oxidized in dry air at: (□) 600 °C, (+) 550 °C, (○) 500 °C, and (◇) 450 °C.

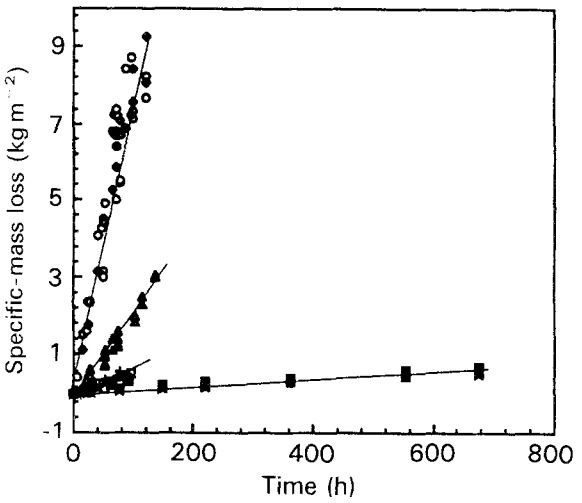

Figure 18 Comparison of oxidation data for unidirectional and $[0/90]_{2s}$ 1723 composites: (□) unidirectional, 500 °C; (+) $[0/90]_{2s}$ 500 °C; (○) unidirectional, 600 °C; (◆) $[0/90]_{2s}$, 600 °C; (▲) unidirectional; 550 °C; (△) $[0/90]_{2s}$, 550 °C; (*) unidirectional; 450 °C; (■) $[0/90]_{2s}$, 450 °C.

that can be attributed to differences in composite lay-up. This is not the case with the 7740 composites.

Figs 19–22 show plots of specific-mass loss versus time for the unidirectional 7740 composites. (Four different graphs are shown because of scatter in the data.) In this instance, the data are not linear with time, but exhibit parabolic behaviour. The significance of this will be discussed later.

To calculate an effective oxidation activation energy for these weight-loss measurements, best-fit lines were drawn through data points taken at longer oxidation times, as the curve tends to level off at longer oxidation exposures. By plotting these slopes as log(slope) against T^{-1} (Fig. 23), an effective activation energy for the oxidation of carbon fibres in a unidirectional 7740 composite was determined to be 169 kJ mol^{-1}, which is consistent with the activation energy for the oxidation of the bare fibres (176 kJ mol^{-1}), allowing for experimental error.

Fig. 24 shows a plot of specific-mass loss against time for $[0/90]_{2s}$ 7740 composites tested at 450, 500, 550, and 600 °C. Once again, these data are parabolic with time. The data show an initial rapid oxidation

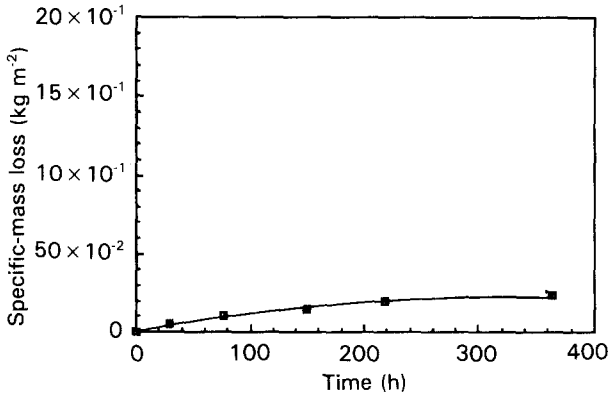

Figure 19 Plot of specific-mass loss for 7740 unidirectional composites oxidized at 450 °C.

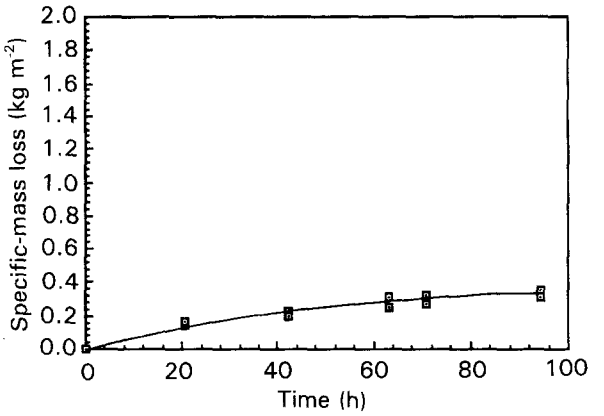

Figure 20 Plot of specific-mass loss for 7740 unidirectional composites oxidized at 500 °C.

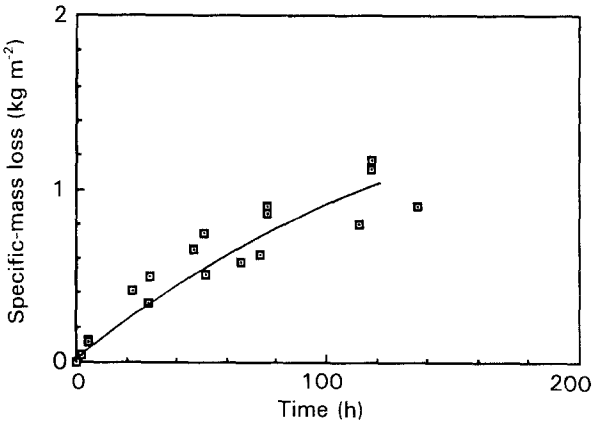

Figure 21 Plot of specific-mass loss for 7740 unidirectional composites oxidized at 550 °C.

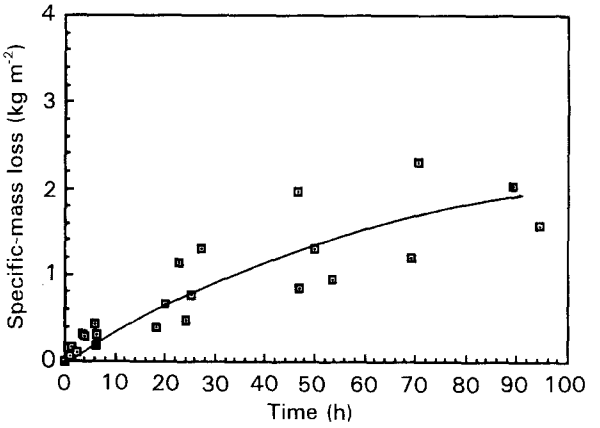

Figure 22 Plot of specific-mass loss for 7740 unidirectional composites oxidized at 600 °C.

rate; however, at approximately 25 h the oxidation rate decreases. This phenomenon is particularly pronounced at 550 and 600 °C. This change in slope is not caused by fibre depletion, since even at 600 °C, only 15–20% of the fibres have been consumed after 25 h. Additionally, this phenomenon is more pronounced in the $[0/90]_{2s}$ 7740 composites than in the unidirectional 7740 material, and it does not occur at all in the 1723 composites. This phenomenon of parabolic oxidation behaviour can be caused by two different events. Either the fibres are being depleted in the matrix, thereby reducing the amount of carbon available for chemical reaction with oxygen, or the amount of carbon-fibre-surface area is being reduced as a function of time. Even in the $[0/90]_{2s}$ 7740 material, which oxidizes much more rapidly than the unidirectional 7740 composites at 600 °C, approximately 80% of the fibres have not undergone a chemical reaction when the curve begins to flatten (after 25 h). The decelerating oxidation rate is also not caused by a mass-transport process (see Section 6.5). Thus, the decrease in oxidation rate is caused by a reduction in available fibre-surface area. This reduction in surface area can be caused by two different factors: either the capillaries created by fibre recession from the edges of the composite or the cracks caused by thermal mismatch heal over time. Fig. 25 shows a scanning electron micrograph of the edge of a $[0/90]_{2s}$ 7740 composite which was oxidized for 165 h at 600 °C.

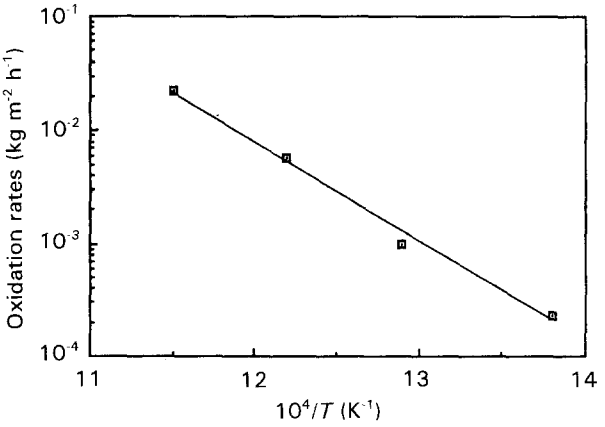

Figure 23 Plot of log(oxidation rate) versus T^{-1} for the oxidation data in Figs. 19–22 showing an Arrhenius-type relationship.

From this micrograph, it is evident that the glass has not flowed into the capillaries created by fibre recession. The original imprint of the fibre can be seen in the glass. In addition, there is no rounding of the edges created by the fibre/matrix interface, which is further evidence that the glass did not flow.

In the next section, microstructural evidence will be presented to show that the cracks produced by thermal mismatch do indeed heal due to the elevated

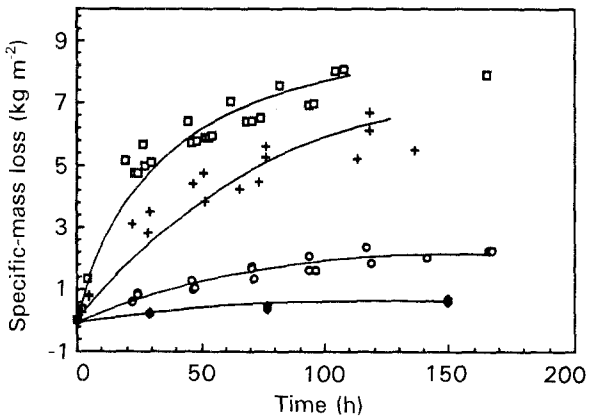

Figure 24 Plot of specific-mass loss for 7740 $[0/90]_{2s}$ composites oxidized at: (□) 600 °C, (+) 550 °C, (○) 500 °C, (◇) 450 °C.

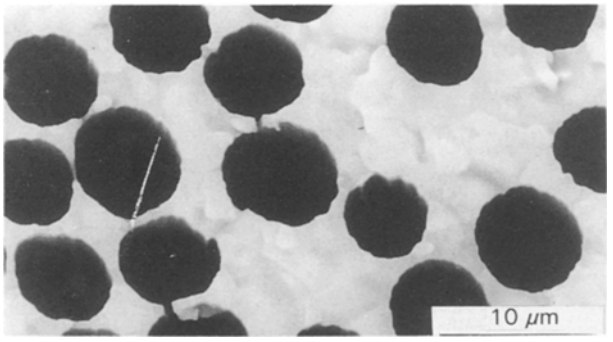

Figure 25 SEM micrograph of the edge of a $[0/90]_{2s}$ composite that was oxidized for 165 h at 600 °C.

temperature exposure. Since the cross-plied composites have a higher volume fraction of cracks, they oxidize more rapidly than the unidirectional material; however, as time proceeds, these cracks close, and the oxidation rate of the cross-plied composites approaches that of the unidirectional material. This effect is more pronounced in the 7740 composites than in the 1723 material because the 7740 glass has a much lower glass-transition temperature. At 600 °C, the temperature is in excess of the T_g for 7740 glass; therefore, the glass can undergo viscous flow. Viscous flow occurs preferentially at the crack tip rather than at the capillaries created by fibre recession because the crack tip has a much higher chemical potential than the cylinders created by oxidation of the fibre ends in the composite.

6.3. Microstructural evidence of matrix microcracking in composites

Matrix microcracks caused by thermal mismatch are created in the initial hot pressing of the as-infiltrated plies, and possibly by the thermal cycling the composite experiences during oxidation testing. Fig. 26 shows the surface of an as-received 7740 unidirectional composite. The cracks are not readily visible in this condition. Upon oxidizing, more cracks may form, and the cracks become more visible as seen in Fig. 27, which shows a unidirectional 7740 composite

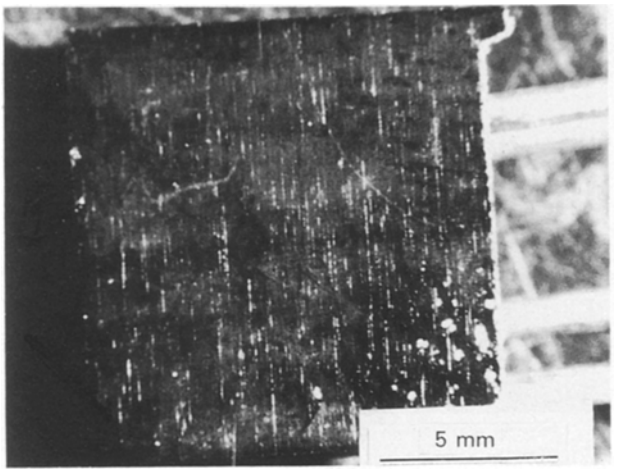

Figure 26 Macrograph of an as-hot-pressed 7740 unidirectional composite sample.

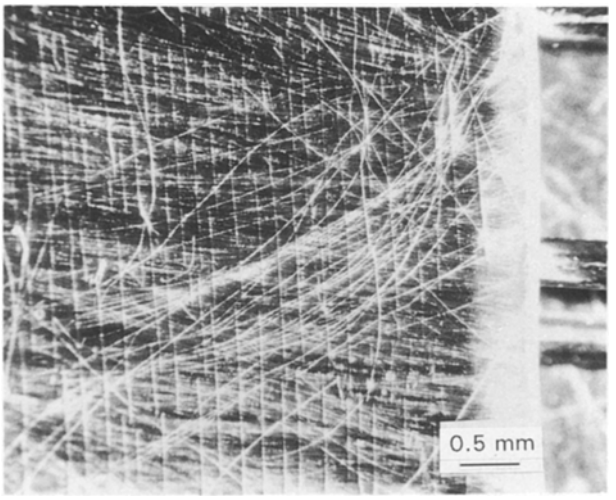

Figure 27 Macrograph of an oxidized unidirectional 7740 sample (89 h at 600 °C) showing matrix microcracking.

which has been oxidized for 89 h at 600 °C in air. The cracks are tinted during the oxidation process.

Fig. 28 shows the cracking pattern in a $[0/90]_{2s}$ 7740 composite which has been oxidized for 94 h at 600 °C. Rather than spanning the width of the sample, these cracks form a grid pattern. The shear stresses created by the $[0/90]_{2s}$ lay-up have an obvious effect on the cracking behaviour of the matrix. Likewise, cross-plying also creates a higher volume fraction of cracks in the 7740 composites (see Table IV).

In the 1723 composites, the matrix microcracks are not as readily visible. At elevated temperatures, light-scattering effects caused by the absence of the fibres make it impossible to view the cracks from the surface of the sample. The cracks are more easily seen in a polished cross-section of the material.

These matrix microcracks do indeed serve as short-circuit diffusion paths by which oxygen can gain access to the carbon fibres. Fig. 29 shows a polished cross-section of a unidirectional 7740 composite which was oxidized at 500 °C for 210 h. Those fibres which intersect the crack are severely degraded, while

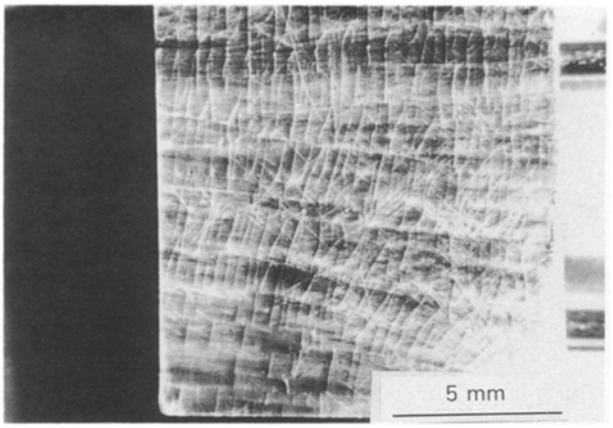

Figure 28 Macrograph of an oxidized 7740 $[0/90]_{2s}$ composite (94 h at 600 °C) showing the cracking pattern created by cross-plying.

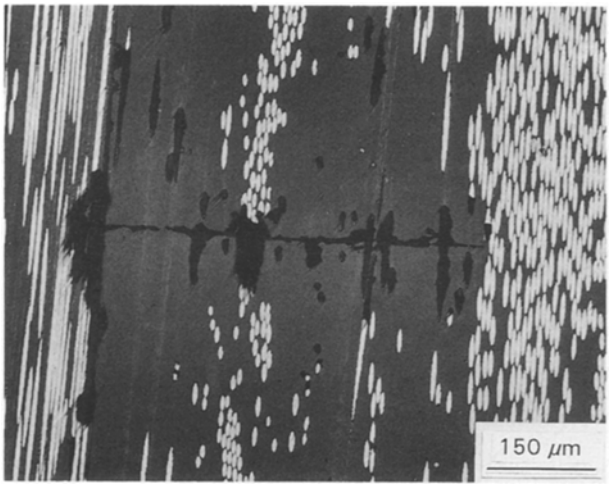

Figure 29 Polished cross-section of a 7740 unidirectional composite oxidized at 500 °C for 210 h.

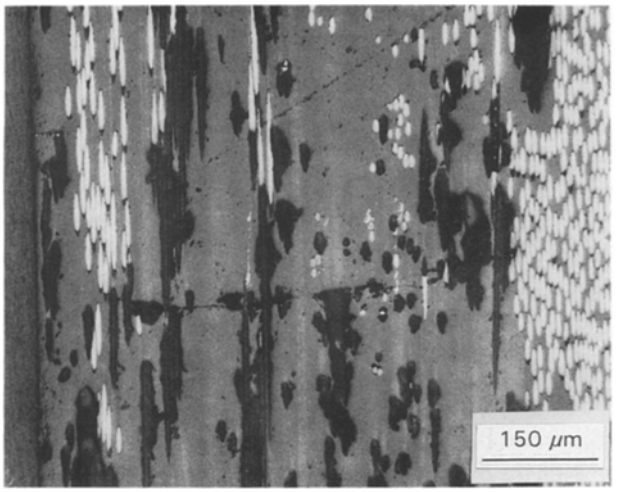

Figure 30 Optical micrograph of an oxidized 1723 unidirectional composite (164 h at 600 °C).

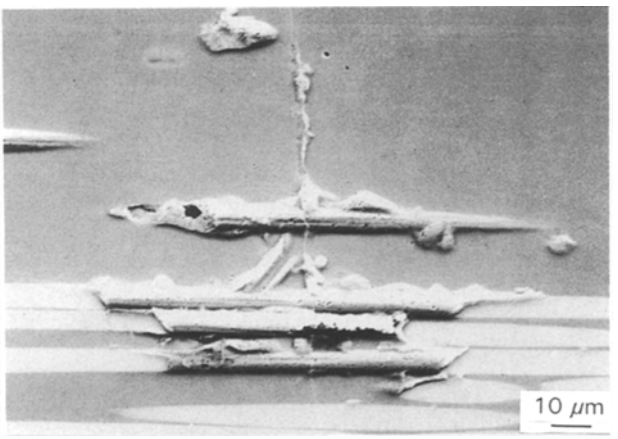

Figure 31 Backscattered SEM micrograph of the sample shown in Fig. 29.

adjacent fibres are completely unreacted. This same phenomenon also occurs in the 1723 composites. Fig. 30 shows an optical micrograph of a unidirectional 1723 composite which was oxidized at 600 °C in dry air for 164 hours. Those fibres which intersect a crack are oxidized, while those embedded in the uncracked matrix are intact.

Fig. 31 shows a backscattered SEM micrograph of the sample shown in Fig. 29. The white bands are unoxidized fibres, while the features showing a relief effect are capillaries which were once occupied by fibres. Fig. 32 shows a high-magnification micrograph of a matrix/fibre intersection. From this micrograph, it can be seen that the fibre does not pull away from the fibre/glass interface.

Fig. 33 shows a crack which has intersected several fibres and then appears to pinch off at the crack tip (500 °C, 210 h). This may be caused by a stress–relaxation effect whereby at elevated temperatures, there is insufficient stress to promote additional crack growth, and the crack has simply stopped; or that at elevated temperatures, there was sufficient time and energy for the glass to flow locally, thereby closing the crack.

Figure 32 High-magnification micrograph of a matrix/fibre interface.

Fig. 34 shows a macrograph of a unidirectional 7740 composite which was oxidized at 600 °C for 47 h. This macrograph shows the widespread damage caused by the matrix microcracking. The white regions are locations where oxygen has been transported along a matrix microcrack, and has then oxidized the fibres parallel to the fibre axis.

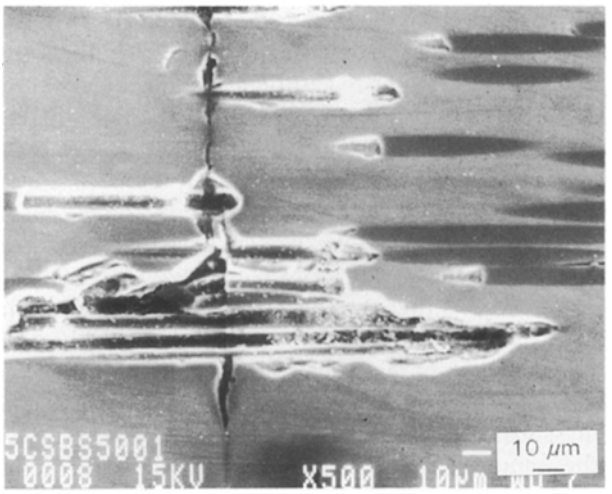

Figure 33 SEM micrograph of a crack that has intersected several fibres and pinched off.

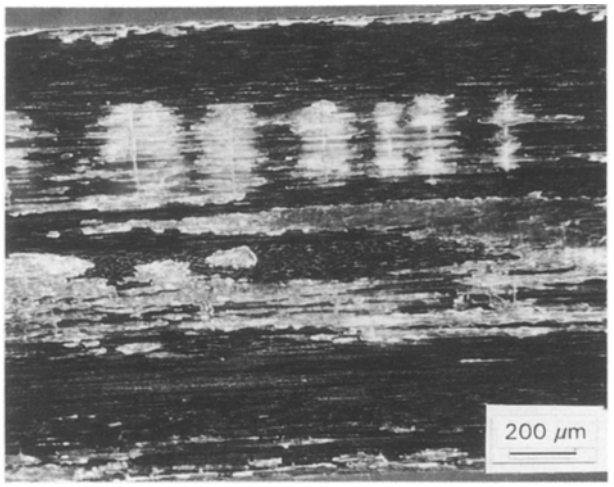

Figure 34 Macrograph of a 7740 unidirectional composite that was oxidized for 47 h at 600 °C.

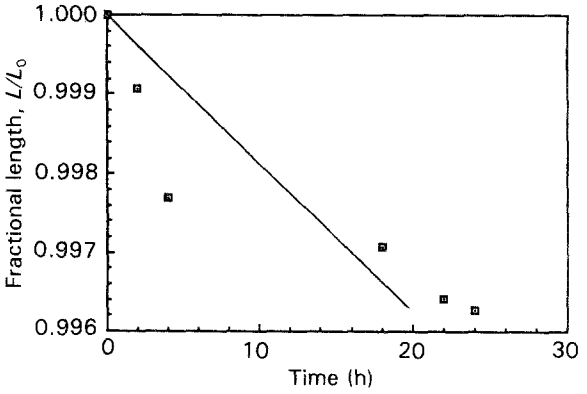

Figure 35 Plot of fibre-end recession against time for 7740 unidirectional composites oxidized at 600 °C.

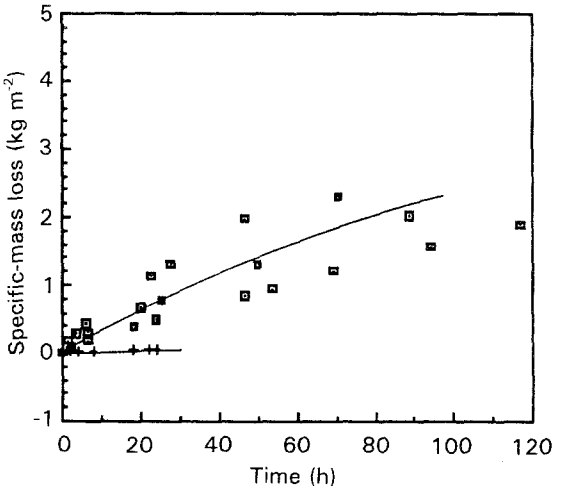

Figure 36 Plot of specific-mass loss from end-recession measurements, and total mass loss for 7740 unidirectional composites oxidized at 600 °C: (□) composites, and (+) mass loss from ends.

6.4. Measurement of fibre recession in unidirectional composites

There are three operative transport mechanisms involved in the oxidation of the carbon fibres contained in carbon-fibre/glass-matrix composites: (i) bulk transport of diffusing species through the glass matrix, (ii) transport along the capillaries once occupied by carbon fibres, and (iii) diffusion along matrix microcracks. Parameters (i) and (iii) are not easily measured. Item (ii) however, can be monitored using a rather direct method.

Unidirectional 7740 composite samples were oxidized at 600 °C in dry air for a given length of time. The samples were removed from the furnace, and were sectioned parallel to the fibre direction. After metallographic preparation, the samples were photographed. The depth of recession was measured using an optical planimeter. Accelerated fibre recession occurred at the corners of the samples caused by overlapping diffusion fields. This accelerated effect was not included in these measurements. Fig. 35 shows a plot of the data obtained from these measurements, plotted as recession distance against time.

Knowing the volume fraction and the density of the fibres, this distance measurement can be converted into a mass loss as shown in Fig. 36, plotted as specific-mass loss versus time. Fig. 36 also shows oxidation data for a typical unidirectional 7740 composite. The comparison of these data reveals that weight loss due to fibre recession is not the dominant weight-loss mechanism. At longer times, fibre recession contributes only a minimal fraction of the total weight loss.

6.5. Transport mechanisms involved in the oxidation of carbon-fibre/glass-matrix composites

One of the recurring ideas or phenomena in this investigation is mass transport. Knowing how the oxidation products and reactants are transported in the interior of the composite is crucial to understanding the overall oxidation process of the material.

To date, no data has been obtained on the solid-state diffusion of oxygen or carbon-dioxide glasses. The vast majority of diffusivity values are for helium and water in glass. These data are unsuitable for application in this study because helium diffuses orders of magnitude faster than other gases because of its small atomic radius, and water reacts with most glasses while diffusing. The only available data on

oxygen diffusion in glass is for the diffusion of oxygen-18 in a glass melt of SiO_2–20 mol % Na_2O [18]. If these are extrapolated to 600 °C, the diffusivity of oxygen is approximately 6×10^{-13} cm^2 s^{-1}. Thus, solid-state diffusion is far too slow for it to be considered a viable mechanism for oxygen transport.

In the absence of solid-state diffusion, all material transport must occur in the gaseous state, either through the matrix microcracks or the capillaries created by end recession of the fibres. If the capillaries or cracks are sufficiently small for the collisions between a gaseous molecule(s) and the channel wall to affect the transport process, then Knüdsen diffusivity must be applied. For this to occur, the mean free path of the diffusing species must be of the same order of magnitude as the capillary diameter. However, if this does not occur, unaltered gas kinetics are applicable. In this study, the capillary diameter is ~7 μm, and the calculated mean free path of oxygen, λ, at 600 °C is ~0.3 μm. Therefore, it can be assumed that Knüdsen diffusion is not applicable.

The interdiffusivity, D_{AB}, of two gaseous molecules, A and B, of unequal size, can be expressed by the following equation [19]:

$$D_{AB} = \frac{2}{3}\left(\frac{K_B^3}{\pi^3}\right)^{1/2}\left(\frac{1}{2m_A} + \frac{1}{2m_B}\right)^{1/2}\left(\frac{T^{3/2}}{\frac{1}{4}P(d_A + d_B)^2}\right) \quad (2)$$

where d is the molecular diameter, m is the molecular mass, k_B is Boltzmans constant, T is the absolute temperature, and P is the pressure.

In this application, A is oxygen (O_2) and B is carbon monoxide (CO) or carbon dioxide (CO_2). At 600 °C and a pressure, P, equal to the partial pressure of oxygen (0.2 atm), the interdiffusion coefficient, D_{AB}, of CO and O_2 is ~3.0 cm^{2}s^{-1} and the interdiffusion coefficient of CO_2 and O_2 is ~2.0 cm^{2}s^{-1}.

In very small matrix microcracks, (0.01–1 μm) Knüdsen diffusivity may have a measurable effect on gaseous transport, and can be expressed as

$$D_{kn}(\text{cm}^2\,\text{s}^{-1}) = 9700\,r\left(\frac{T}{M}\right)^{1/2} \quad (3)$$

where r is the crack width (cm), T is the absolute temperature, and M is the molecular weight of the diffusing species (g mol^{-1}).

For a diameter of 0.01 μm at 600 °C, the diffusivity of oxygen would be 0.05 cm^2 s^{-1}, and for a diameter of 1 μm, the diffusivity of oxygen is 5.1 cm^2 s^{-1}. Therefore, only in very small cracks would Knüdsen diffusivity play a role in the mass transport of oxygen. In most instances, the crack diameter is approximately the same size as the fibre diameter (7 μm). Therefore, Knüdsen diffusivity is not rate limiting, and gaseous transport does not control the oxidation of the fibres in the glass matrix.

6.6. Comparison of composite and fibre-oxidation data

At the inception of this study, one of the primary goals was to make a direct comparison between the oxidation behaviour of the bare carbon fibres and the fibres in the composites to determine if, by placing the fibres in a glass matrix, the oxidation mechanism(s) changed. Additionally, this study was to also determine whether or not the glass matrix provided an intrinsic increase in oxidation resistance in the fibres. It has been shown that the oxidation of fibres, both unprotected and in the two glass matrices, has an effective oxidation activation energy of approximately 174 kJ mol^{-1}. This indicates that the chemical reactions involved in the oxidation process do not change between the bare fibres and the fibres in the composite. It is impossible, however, to directly compare the values of specific mass-loss versus time for the bare fibres and fibres in the composites because the scaling factor of the initial exposed surface area is not a true value for the surface area that is being oxidized. In the bare fibres, the oxidation process is not uniform in the entire bundle, but occurs from the outside of the fibre tow inward. In the composites, the amount of surface area created by crack/fibre intersections is unknown. Thus, no absolute comparisons should be made beyond what has already been stated.

A gross comparison of the fibre and composite data can be made, however, by replotting the data already presented as a mass fraction (mass at time t/initial mass) against time, thereby side-stepping the concept of available surface area. If this is done, it is evident that for all the composites at all of test temperatures examined in this investigation, the fibres in the glass matrices oxidize more slowly than the bare fibres. Figs 37–39 show the best-fit lines for mass fraction versus time for bare fibres and the fibres in unidirectional 1723 composites oxidized at 500, 550 and 600 °C in dry air. Data points are not shown because the scatter and number of data points would make such a comparison rather cluttered.

From Figs 37–39, it is evident that the glass does provide some oxidation resistance to the fibres; however, this protection is not as significant as expected. With a small volume fraction of matrix microcracks, the oxidation rates of the bare fibres and the fibres in

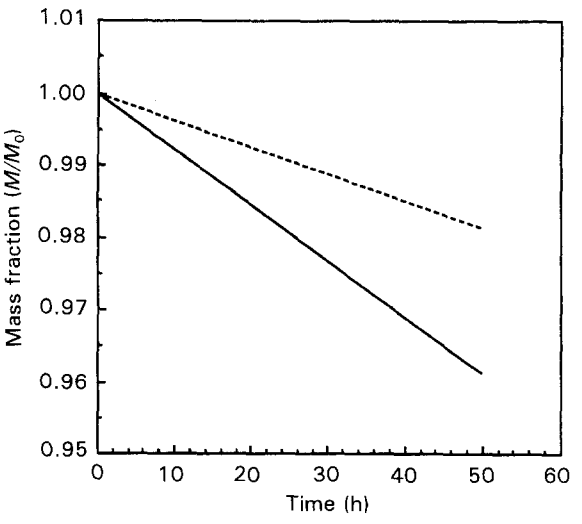

Figure 37 Plot of mass fraction against time for the oxidation at 500 °C of: (– – –) unidirectional 1723 composites, and (——) bare fibres.

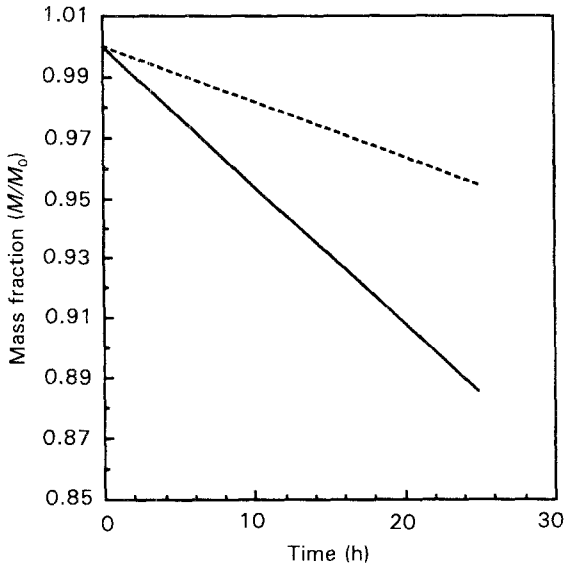

Figure 38 Plot of mass fraction against time for the oxidation at 550 °C of: (– – –) unidirectional 1723 composites, and (——) bare fibres.

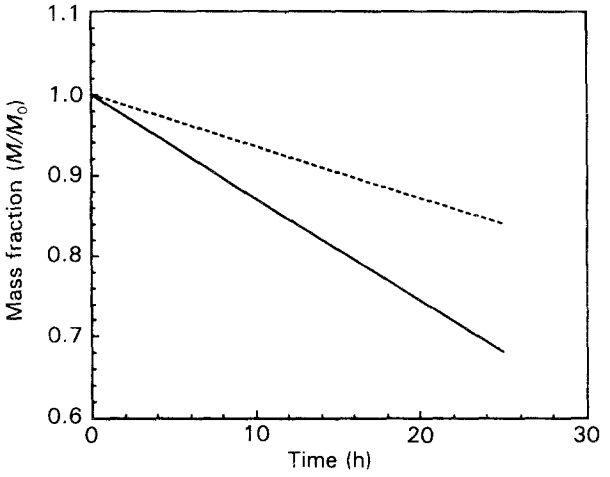

Figure 39 Plot of mass fraction against time for the oxidation at 600 °C of: (– – –) unidirectional 1723 composites and (——) bare fibres.

the 1723 composites are within one order of magnitude, even at 600 °C. These cracks must be eliminated before this class of composite can be used in industrial applications.

7. Conclusions

1. The oxidation of carbon fibres is controlled by the amount of available surface area.

2. The activation energy for the fibres used in this investigation was found to be 174 kJ mol^{-1}, which is in good agreement with other commercially produced PAN-based fibres.

3. The activation energy for the carbon fibres does not change once the fibres are placed within a glass matrix, indicating that the oxidation mechanism does not change when the fibres are used in composites.

4. Oxygen transport through matrix microcracks is the main mode of oxygen transport in the composites used in this investigation.

5. When a composite is oxidized near or above the glass-transition temperature of the matrix the microcracks heal, thereby decreasing the amount of available surface area, and slowing the rate of oxidation.

6. Transport of oxygen in these composites can be adequately described by traditional gas kinetics.

References

1. I. CRIVELLI-VISCONTI and G. A. COOPER, *Nature* **221** (1969) 754.
2. R. A. J. SAMBELL, D. G. BOWER and D. C. PHILLIPS, *J. Mater. Sci.* 7 (1972) 663.
3. R. A. J. SAMBELL, A. BRIGGS, D. C. PHILLIPS and D. H. BOWEN, *J. Mater. Sci.* 7 (1972) 676.
4. D. C. PHILLIPS, F. A. J. SAMBELL and D. H. BOWEN, *J. Mater. Sci.* 7 (1972) 1454.
5. S. R. LEVITT, *J. Mater. Sci.* **8** (1973) 793.
6. K. M. PREWO, *Mater. Sci. Res.* **20** (1986) 529.
7. E. FITZNER, A. GKOGKIDIS and M. HEINE, *High Temperatures–High Pressures* **16** (1984) 363.
8. K. K. CHAWLA, *J. Met.* **35**(3) (1983) 82.
9. S. C. BENNETT, D. J. JOHNSON and W. JOHNSON, *J. Mater. Sci.* **8** (1983) 3337.
10. D. J. JOHNSON, Chemistry and Physics of Carbon, Vol.20, edited by P. A. Thrower (Marcel Dekker, New York, 1987) p. 1.
11. B. L. BUTLER and R. J. DIEFENDORF, in Papers of the 9th Conference on Carbon, June 16–20, 1969, Boston, MA (American Carbon Society, University Park, PA, 1969) p. 45.
12. B. J. WICKS and R. A. COYLE, *J. Mater. Sci.* **11** (1976) 376.
13. N. P. BANSAL and R. H. DOREMUS, "Handbook of glass properties" (Academic Press, Orlando, 1986) pp. 32–37.
14. K. M. PREWO, J. J. BRENNAN and G. K. LAYDEN, *Ceram. Bull.* **65(5)** (1986) 305.
15. B. H. ECKSTEIN, "The weight loss of carbon fibres in circulating air", 18th International SAMPE Biennial Conference, 7–9 October 1986, Seattle, Washington (SAMPE, Covina, CA, 1986) p. 149.
16. J. B. BARR and B. H. ECKSTEIN, "The oxidation of carbon fibres in air", Extended Abstract of the 18th Biennial Conference on Carbon (Worcester, MA, 1987).
17. CLYDE H. SHEPPARD, "Thermal and oxidative stability of carbon fibres and composites", 18th International SAMPE Technical Conference, 7–9 October, 1986, Seattle, Washington (SAMPE Covina, CA, 1986) pp. 142–148.
18. Y. OISHI, R. TERAI and H. UEDA, "Mass transport phenomenon in ceramics", edited by A. R. Cooper and A. H. Heuer (Plenum, New York, 1975) p. 297.
19. G. H. GEIGER and D. R. POIRIER, "Transport phenomena in metallurgy" (Addison-Wesley, Reading, MA, 1973) pp. 464–469.

Received 28 July
and accepted 26 October 1992